JOURNAL OF MATERIALS SCIENCE **35** (2000) 2093–2097

Dielectric properties of PFW-PMN relaxor system prepared by B-site precursor method

S. G. JUN, N. K. KIM
Department of Inorganic Materials Engineering, Kyungpook National University, Taegu, South Korea, 702-701
E-mail: nkkim@kyungpook.ac.kr

Phase-pure perovskite powders in the $Pb(Fe_{2/3}W_{1/3})O_3$-$Pb(Mg_{1/3}Nb_{2/3})O_3$ system were synthesized by a B-site precursor method and were densified into ceramic form. Lattice parameter changes were examined as a function of composition. Sinterability was studied by measuring bulk densities of the fired ceramic specimen. Composition- and frequency-dependent weak-field dielectric properties in the low frequency range are reported. Curie temperatures shifted linearly with composition change, while the maximum dielectric constants did not show a linear relationship. © *2000 Kluwer Academic Publishers*

1. Introduction

Lead-based complex perovskite compounds, $Pb(B',B'')O_3$, have been investigated widely as chip capacitor dielectrics, due to their low-temperature sinterability, high dielectric constants with broad dielectric spectra (diffuse phase transition, DPT), low electric field dependency, etc. The DPT behaviors are frequently observed in complex perovskite compounds and ferroelectric solid solutions, and are considered to be originating from local compositional fluctuation, which indicates that chemical inhomogeneity at the B-sites of a perovskite structure influences the phase transition modes [1–3]. Moreover, a number of complex perovskites also exhibit frequency-dependent dielectric relaxation phenomena, and thus are often called relaxors. The dielectric relaxations are typified by decreasing maximum dielectric constants (K_{max}'s) and increasing Curie temperatures (T_C's), maximum dielectric losses, and peak temperatures of the maximum loss, with increasing measurement frequency.

Lead iron tungstate ($Pb(Fe_{2/3}W_{1/3})O_3$, PFW) and lead magnesium niobate ($Pb(Mg_{1/3}Nb_{2/3})O_3$, PMN) are representative relaxor ferroelectrics of cubic disordered perovskite structures (JCPDS 40-374 and 27-1199) and have very high dielectric constants ($K_{max} \simeq 20{,}000$ [4, 5] and 18,000 [1, 4, 5]) at $T_C = -95°C$ [6–9] and $-10°C$ [4, 10, 11], respectively. PFW has been studied extensively from the late 70's, in solid solutions with $Pb(Fe_{1/2}Nb_{1/2})O_3$ (PFN) [12–16]) and with $Pb(Fe_{1/2}Ta_{1/2})O_3$ [17]. PMN is one of the most widely studied relaxor ferroelectric compounds due to the very high maximum dielectric constant with DPT behaviors, properly-ranged Curie temperature, superior electromechanical and electrostrictive properties, etc. Potential applications of PMN (and modified compositions thereof) include chip capacitors [4, 5], piezoelectric transducers [18], actuators [19, 20], pyroelectric bolometers [21], etc.

In the present study, two distinct ferroelectric relaxor compounds of PFW and PMN (the former with $B^{3+}_{2/3}B^{6+}_{1/3}$ and the latter with $B^{2+}_{1/3}B^{5+}_{2/3}$ B-site ion complexes) were chosen. Selected compositions in the PFW-PMN pseudobinary system (with four different ions of Mg^{2+}, Fe^{3+}, Nb^{5+}, and W^{6+}, all with different valences, competing at the 6-fold octahedral sites of a perovskite structure) were prepared as ceramics and characterized in terms of phase development, lattice parameters, sinterability, and dielectric properties. In order to suppress the formation of harmful pyrochlores and thereby to enhance the perovskite phase yields for better dielectric properties, the B-site precursor method (more comprehensive term for the so-called columbite process [22]) was used, where PbO is reacted with precalcined product of B-site precursor powders, details of which can be found elsewhere [16, 17].

2. Experimental

The system under investigation is $(1-x)Pb(Fe_{2/3}W_{1/3})O_3$-$xPb(Mg_{1/3}Nb_{2/3})O_3$(i.e., $Pb(Mg_{x/3}Fe_{2(1-x)/3}Nb_{2x/3}W_{(1-x)/3})O_3$ or $(1-x)$PFW-xPMN), where x changed from 0.0 to 1.0 at regular intervals of 0.2. Raw materials used were PbO (99.5% purity), MgO (99.9%), Fe_2O_3 (99.99%), Nb_2O_5 (99.9%), and WO_3 (>99%). Moisture contents of raw chemicals and synthesized B-site precursors were measured and introduced into the batch calculations, in order to preclude effects of adsorbed moisture. To synthesize B-site precursor powders of $(Mg_{x/3}Fe_{2(1-x)/3}Nb_{2x/3}W_{(1-x)/3})O_2$ (i.e., $(1-x)(Fe_{2/3}W_{1/3})O_2$-$x(Mg_{1/3}Nb_{2/3})O_2$ composition, all constituent oxides were weighed in appropriate proportions, wet-mixed under alcohol with ZrO_2 milling media, dried, and were calcined at 950°–1150°C for 2 h in air. Stoichiometric amounts of PbO were then added to the prepared B-site precursors, mixed, and were calcined at 750°–850°C for 2 h to develop perovskite

structures. During the syntheses of B-site precursor and perovskite powders, double calcinations were carried out (if necessary) to enhance the formation yields of desired phases, which were monitored by powder x-ray diffraction (XRD) using Cu K_α radiation. Perovskite phase yields were determined by comparing x-ray intensities of major diffraction peaks, i.e., (110) of perovskite and (222) of pyrochlore structures. Lattice parameters of the perovskite structures were determined by using the Cohen's method. Pellet-type samples (10 mm in diameter and ∼1 mm thick) were uniaxially pressed using the perovskite powders granulated with polyvinylalcohol binder (2 wt% dilute solution for ready dispersion) and were further compacted isostatically at 100 MPa. In order to prevent lead loss during sintering, pellets were embedded in atmosphere powder of identical perovskite composition and were fired in a double-crucible setup [23] at 800°–1250°C for 1 h. Bulk densities of the sintered specimens were measured geometrically, after grinding and polishing to attain parallel sides. After gold sputtering on major faces of samples, dielectric constant and loss characteristics were investigated in the temperature range of −150°–180°C on cooling, using a computer-interfaced impedance analyzer (10^{3-6} Hz, oscillation level = 1 V_{rms}).

3. Results and discussion

In Fig. 1 are x-ray profiles of the B-site precursor system, $(1-x)(Fe_{2/3}W_{1/3})O_2$-$x(Mg_{1/3}Nb_{2/3})O_2$ (i.e., $(1-x)Fe_2WO_6$-$xMgNb_2O_6$), where end components of $x = 0.0$ and 1.0 showed corresponding patterns Fe_2WO_6 and $MgNb_2O_6$ (columbite phase), as contrasted in Fig. 2. Although intermediate compositions possessed diffraction peaks varying between those of Fe_2WO_6 and $MgNb_2O_6$ in general, several extraneous peaks (e.g., most noticeably at $2\theta \simeq 23.8°$), however, do not fit into such a relation. Instead, the x-ray pattern of $MgWO_4$ (Fig. 2) seems to fit quite satisfactorily with those of intermediate compositions. Then also arises a possibility of $FeNbO_4$ (wolframite structure) formation, which actually appeared to occur. Therefore diffraction peaks of $FeNbO_4$ and $MgWO_4$ are denoted at $x = 0.4$ and 0.6 in Fig. 1, respectively, which does not necessarily mean that x-ray spectra of corresponding compositions matched exactly with those of $FeNbO_4$ and $MgWO_4$.

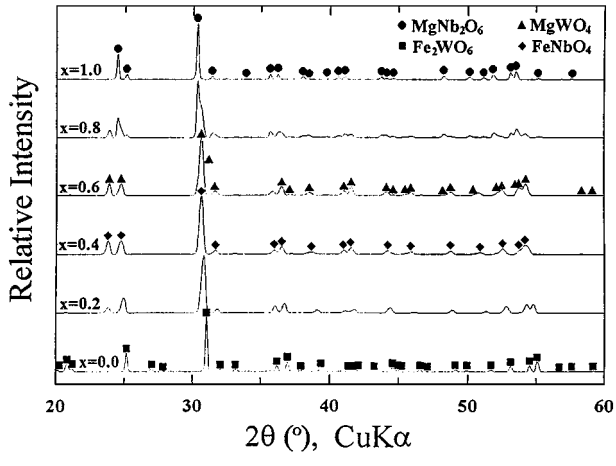

Figure 1 Room temperature x-ray diffraction patterns of B-site precursor system $(1-x)Fe_2WO_6$-$xMgNb_2O_6$.

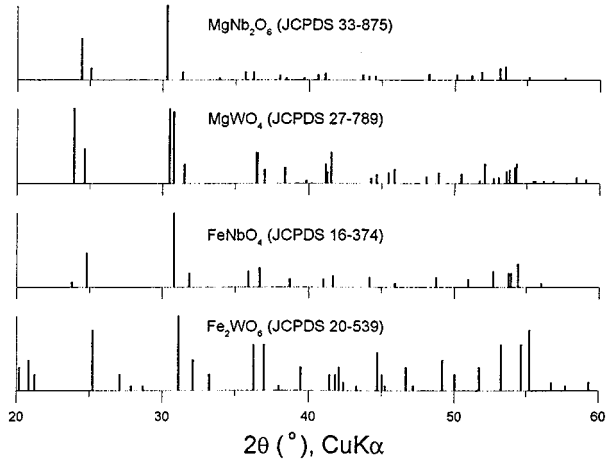

Figure 2 Comparison among diffraction profiles of $MgNb_2O_6$, $MgWO_4$, $FeNbO_4$, and Fe_2WO_6.

As Fe_2WO_6 and $MgNb_2O_6$ have somewhat different profiles, e.g., absence of three diffraction lines at 20–21° in $MgNb_2O_6$ and profile displacements by ∼1° in 2θ (Fig. 2), Fe_2WO_6 did not seem to be isostructural with columbite $MgNb_2O_6$. Meanwhile, profiles of $FeNbO_4$ and $MgWO_4$ are quite similar each other, except for the drastic differences in intensity of the peaks at ∼24° and other minor details (Fig. 2). The structure developments of $FeNbO_4$ and $MgWO_4$ (possibly along with Fe_2WO_6 and $MgNb_2O_6$) at intermediate compositions seem to be arised by the too complex nature of the B-site ions of 1:2 and 2:1 combinations of $MgNb_2O_6$ and Fe_2WO_6, where valences of B′ and B″ ions are 2+ or 3+ and 5+ or 6+, respectively. Such complexities might have caused favoring for the simpler ratio of 1:1 in $FeNbO_4$ and $MgWO_4$. In a similar but less complicated case of a perovskite system $Pb(Mg_{1/3}Ta_{2/3})O_3$-$Pb(Zn_{1/3}Nb_{2/3})O_3$ [23] with four different species of B-site ions (but only with 1:2 combinations of Mg^{2+} or Zn^{2+} and Ta^{5+} or Nb^{5+}), whether intermediate compositions developed $MgNb_2O_6$ and $ZnTa_2O_6$ (instead of $MgTa_2O_6$ and $ZnNb_2O_6$) could not be determined clearly, as x-ray profiles of $MgNb_2O_6$ and $ZnTa_2O_6$ are isostructural with $ZnNb_2O_6$ (columbite structure) and diffraction angles are almost identical, too.

X-ray spectra of the perovskite system $(1-x)$PFW-xPMN are displayed in Fig. 3. The system formed continuous crystalline solutions of a perovskite structure with only trace amounts of pyrochlores (perovskite phase yield ≥ 99.4%). As superlattice reflections were not detected at all in the entire composition range, any structural ordering among the four B-site species does not appear to occur (at least in the macroscopic scale), so the whole compositions are expected to show DPT behaviors. In Fig. 4 are lattice parameters of the perovskite structure, as determined from the x-ray patterns in Fig. 3, with barely detectable non-perovskite peaks manually discriminated. Lattice parameters of PFW and PMN were 0.3985 and 0.4046 nm Å, very close to the reported data [10, 12, 24, 25]. The gradual

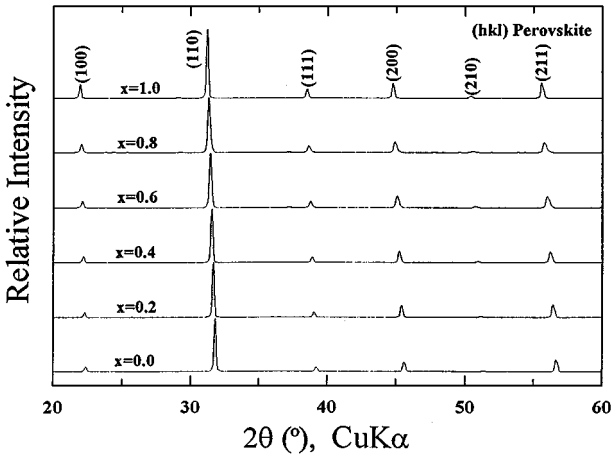

Figure 3 Room temperature x-ray diffraction patterns of $(1-x)$ $Pb(Fe_{2/3}W_{1/3})O_3$-xPb $(Mg_{1/3}Nb_{2/3})O_3$ system.

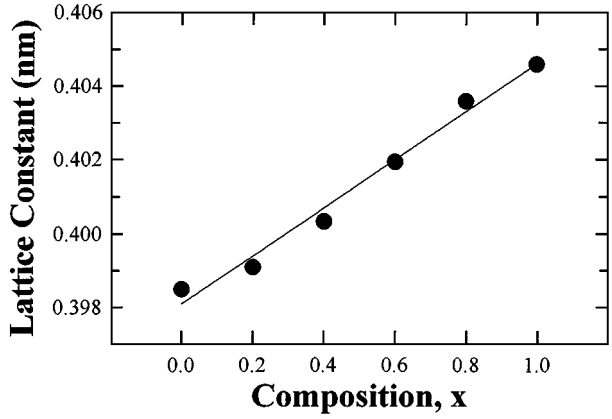

Figure 4 Variation of lattice parameters in the system $(1-x)$PFW-xPMN.

increase of the parameters (as expected from the steady decreases in 2θ of diffraction peaks with increasing x (Fig. 3) or also expected from the average sizes of 0.0630 vs. 0.0667 nm Å [26] for $Fe_{2/3}W_{1/3}$ and $Mg_{1/3}Nb_{2/3}$ octahedral cations) satisfies the Vegard's law, thus the perovskite system PFW-PMN was confirmed to develop complete solid solubility.

Variation of bulk density, as functions of composition and sintering temperature, are presented in Fig. 5.

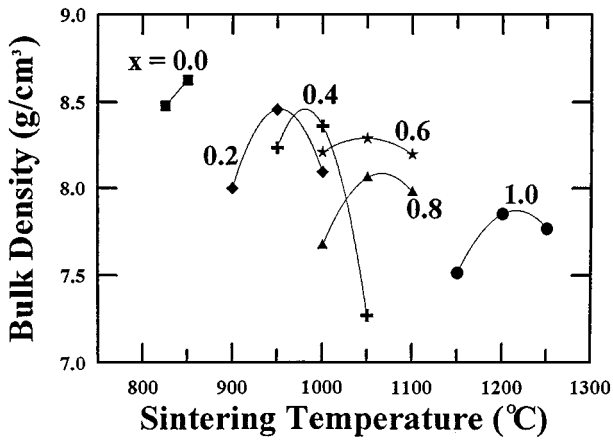

Figure 5 Dependence of bulk densities of $(1-x)$PFW-xPMN ceramics upon sintering temperature.

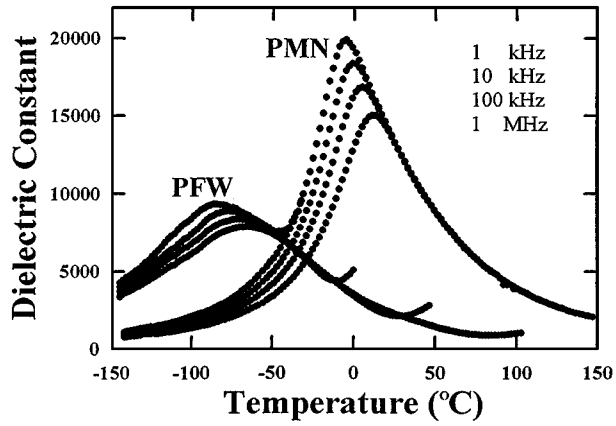

Figure 6 Dielectric constants vs. temperature of PFW and PMN, as a function of frequency.

Three data points, with the central one with the highest density, are plotted for each composition. For PFW, however, only two points (even with increments in sintering temperatures of 25°C) were available, as formation of liquid occurred at higher firing temperatures (as reported in a literature [27]) and little degree of sintering with negligible firing shrinkage was observed at lower temperatures, suggesting a very narrow range of sintering temperatures. Gradual decreases in bulk density with increasing PMN content are natural, considering theoretical densities of 9.303 and 8.154 g/cm^3 for PFW and PMN, respectively. Relative densities of the ceramics were 91–96%, with the lowest value observed for $x = 0.0$ (PFW). Meanwhile, steady increases in sintering temperature with increasing x are due to the relatively refractory nature of PMN, as compared with PFW, whose melting temperature was reported to be ∼935°C [28].

Dielectric constant spectra of PFW and PMN ceramics as a function of measurement frequency are shown in Fig. 6. All of the samples (including those of intermediate compositions, not shown here) demonstrated typical dielectric relaxation with DPT behaviors, as expected from the absence of any structural ordering among the four octahedral cations. Maximum dielectric constants and Curie temperatures of PFW and PMN were 8,900 at −78°C and 18,400 at 0°C (@10 kHz), respectively. Meanwhile, dielectric losses (@10 kHz) of PFW and PMN reached maxima of 8.0% and 14.4% at −102°C and −17°C, respectively, ∼20°C lower than corresponding Curie temperatures. The loss of PMN then decreased to steady values of <0.1% at room temperature, but that of PFW decreased to a minimum of 2.8% at −63°C and increased again as high as >70% at −5°C. Whereas maximum dielectric constant of PMN was comparable with the reported value of 18,000 [1, 4, 5], that of PFW was only half as high, which might be due to the low bulk density (∼91%) of the pellet. However, the low density only still does not give a satisfactory explanation, as PMN (with somewhat higher relative density of ∼96%) showed similar dielectric constant to the reported data. Moreover, earlier works [6, 29] reported lower maximum dielectric constant of 6,000–8,700, somewhat smaller than that of the current study. Causes of such a large discrepancy

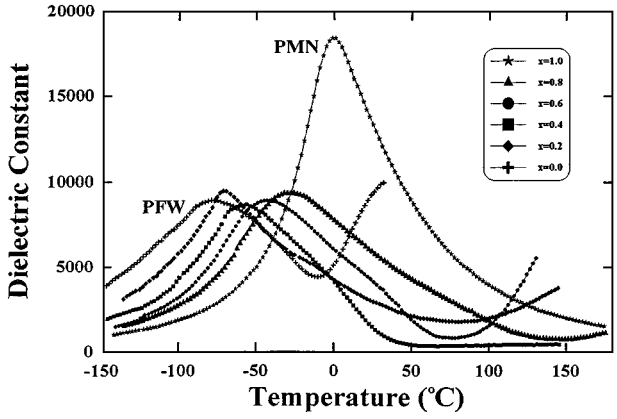

Figure 7 Temperature-dependent dielectric constants in the system $(1-x)$PFW-xPMN (@10 kHz).

need to be studied further. Decrease in maximum dielectric constants with frequency were quantified as K_{max} ratios ($= K_{max,1\,kHz}/K_{max,1\,MHz}$), which are 1.19 for PFW and 1.32 for PMN. In comparison, the values were 1.20 for $Pb(Mg_{1/3}Ta_{2/3})O_3$ [23, 30], 1.25 for $Pb(Fe_{1/2}Ta_{1/2})O_3$ [17], and 1.40 for PFN [16, 31].

Fig. 7 shows dielectric constant spectra of the system $(1-x)$PFW-xPMN, where PMN ($x = 1.0$) showed a maximum dielectric constant of 18,400, while those of all the other compositions ($0.0 \leq x \leq 0.8$) were only half as high, $K_{max} \simeq 8{,}700$–$9{,}500$. Meanwhile, recurrent increases of dielectric constant spectra in the paraelectric region were also observable for PMN-poor compositions, which accompanied enormous increases in dielectric losses. Such dielectric anomalies were frequently observed in lead-based iron- or manganese-containing complex perovskites, e.g., $Pb(Fe_{1/2}Ta_{1/2})O_3$ [17], PFN [16, 31], (Pb,Ca,Sm)(Ti,Mn)O_3 [32], Pb(Zr,Ti)O_3-$BiFeO_3$ [33], etc. and were explained by a space-charge polarization at grain boundary interfaces due to the change of ionic valence from Fe^{3+} to Fe^{2+} [28, 34–36]. Variation of maximum dielectric constants and Curie temperatures of the system are replotted in Fig. 8. All of the Curie temperatures were below room temperature, but still increased continuously with increasing PMN content, verifying formation of complete solid solutions throughout the system. As was discussed in the interpretation of Fig. 7, maximum dielectric constants

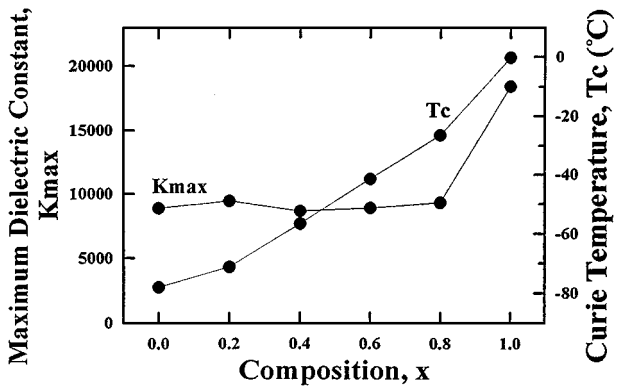

Figure 8 Maximum dielectric constants and Curie temperatures of $(1-x)$PFW-xPMN ceramics (@10 kHz).

remained almost unchanged for $0.0 \leq x \leq 0.8$, but increased nearly twice as high at $x = 1.0$ (PMN). Such an abrupt change in dielectric constants at 20 mol% addition of PFW to PMN is in good contrast to that in the PMN-PFN system [31], where 20 mol% PFN addition to PMN resulted in a slight increase in dielectric constant, while 40–80 mol% addition caused marked increases to ~35,000.

4. Summary

While powders of Fe_2WO_6 and $MgNb_2O_6$ showed corresponding x-ray patterns, intermediate compositions of the B-site precursor system $(1-x)Fe_2WO_6$-$xMgNb_2O_6$ developed mixtures of B′-B″ interchanged phases of $FeNbO_4$ and $MgWO_4$, due probably to the too complex nature of the B-site ion complexes. In contrast, PFW-PMN system formed a series of continuous solid solutions of the perovskite structure, whose lattice parameters increased with increasing PMN content. Optimum sintering temperatures increased, while bulk densities decreased continuously, with increasing PMN content. All of the perovskite compositions showed dielectric relaxation with DPT behaviors. They possessed similar values of maximum dielectric constants (8,700–9,500 @10 kHz), except for PMN with 18,400. Curie temperatures changed gradually with composition.

Acknowledgement

This work was supported by the Korea Science and Engineering Foundation (KOSEF) through the Center for Interface Science and Engineering of Materials (CISEM).

References

1. V. A. BOKOV and I. E. MYL'NIKOVA, *Sov. Phys.-Solid State* **3** (1961) 613.
2. B. N. ROLOV, *Sov. Phys.-Solid State* **6** (1965) 1676.
3. G. A. SMOLENSKII, *J. Phys. Soc. Jpn.* **28** (Suppl.) (1970) 26.
4. Y. SAKABE, in "Proceedings of the MRS International Meeting on Advanced Materials, Vol. 10: Multilayers," Japan, May 1988, edited by M. Doyama, S. Somiya, and R. P. H. Chang (MRS, Pittsburgh, 1989) p. 119.
5. Y. YAMASHITA, *Am. Ceram. Soc. Bull.* **73** (1994) 74.
6. V. A. BOKOV, I. E. MYL'NIKOVA and G. A. SMOLENSKII, *Sov. Phys. JETP* **15** (1962) 447.
7. G. A. SMOLENSKII and V. A. BOKOV, *J. Appl. Phys.* **35** (1964) 915.
8. YU. E. ROGINSKAYA, YU. N. VENEVTSEV and G. S. ZHDANOV, *Sov. Phys. JETP* **21** (1965) 817.
9. S. M. SKINNER, *IEEE Trans. Parts, Materials and Packaging* **PMP-6** (1970) 68.
10. I. G. ISMAILZADE, *Sov. Phys. Cryst.* **5** (1960) 292.
11. K. KATAYAMA, M. ABE, T. AKIBA and H. YANAGIDA, *J. Eur. Ceram. Soc.* **5** (1989) 183.
12. M. YONEZAWA, K. UTSUMI and T. OHNO, in "Proceedings of the 1st Meeting on Ferroelectric Materials and Their Applications," Japan, 1977, p. 297.
13. M. YONEZAWA, K. UTSUMI and T. OHNO, in Proceedings of the 2nd Meeting on Ferroelectric Materials and Their Applications, Japan, 1979, p. 215.
14. H. TAKAMIZAWA, K. UTSUMI, M. YONEZAWA and T. OHNO, *IEEE Trans. CHMT* **CHMT-4** (1981) 345.
15. M. YONEZAWA, *Am. Ceram. Soc. Bull.* **62** (1983) 1375.

16. B.-H. LEE, N.-K. KIM, J.-J. KIM and S.-H. CHO, *Ferroelectrics* **211** (1998) 233.
17. B.-H. LEE, N.-K. KIM, B.-O. PARK and S.-H. CHO, *Mater. Lett.* **33** (1997) 57.
18. S. TAKAHASHI, A. OCHI, M. YONEZAWA, T. YANO, T. HAMATSUKI and I. FUKUI, *Ferroelectrics* **50** (1983) 181.
19. S. J. JANG, K. USHINO, S. NOMURA and L. E. CROSS, *ibid.* **27** (1980) 31.
20. K. UCHINO, *Am. Ceram. Soc. Bull.* **65** (1986) 647.
21. R. E. WHATMORE, P. C. OSBOND and N. M. SHORROCKS, *Ferroelectrics* **76** (1987) 351.
22. S. L. SWARTZ and T. R. SHROUT, *Mater. Res. Bull.* **17** (1982) 1245.
23. M.-C. CHAE, N.-K. KIM, J.-J. KIM and S.-H. CHO, *Ferroelectrics* **211** (1998) 25.
24. A. I. AGRANOVSKAYA, *Bull. Acad. Sci. USSR, Phys. Ser.* **24** (1960) 1271.
25. B. A. MALKOV and YU. N. VENEVESEV, *Inorg. Mater.* **13** (1977) 1189.
26. R. D. SHANNON, *Acta Cryst.* **A32** (1976) 751.
27. N. MIZUTANI, C.-H. LU, K. SHINOZAKI and M. KATO, *J. Am. Ceram. Soc.* **73** (1990) 1214.
28. N. K. KIM and D. A. PAYNE, *J. Mater. Res.* **5** (1990) 2045.
29. V. A. BOKOV and I. E. MYL'NIKOVA, *Sov. Phys.-Solid State* **2** (1961) 2428.
30. M.-C. CHAE and N.-K. KIM, *Ferroelectrics* **209** (1998) 603.
31. S.-G. JUN, N.-K. KIM, J.-J. KIM and S.-H. CHO, *Mater. Lett.* **34** (1998) 336.
32. W. R. XUE, P. W. LU and W. HUEBNER, in "Proceedings of the 9th IEEE International Symposium on Applications of Ferroelectrics," University Park, USA, August 1994, edited by R. K. Pandey, M. Liu and A. Safari (IEEE, 1994) p. 101.
33. W. HUEBNER, W. R. XUE and P. W. LU, in "Proceedings of the 9th IEEE International Symposium on Applications of Ferroelectrics," University Park, USA, August 1994, edited by R. K. Pandey, M. Liu and A. Safari (IEEE, 1994) p. 150.
34. T. R. SHROUT, S. L. SWARTZ and M. J. HAUN, *Am. Ceram. Soc. Bull.* **63** (1984) 808.
35. K. SAKATA and H. TAKAHARA, *Jpn. J. Appl. Phys. Suppl.* **26-2** (1987) 83.
36. N. ICHINOSE and N. KATO, *ibid.* **33** (1994) 5423.

Received 28 July 1997
and accepted 30 September 1999